Supporting Information

Encapsulated Ni nanoparticles in the incomplete graphite layer anchored on NiMo oxides enabling superior hydrogen evolution to Pt

Jiajia Lu,[ad] Peng-Jun Deng,[a] Anyong Chen,[ab] Chen Yang,[ab] Hongwei Zhu[ad] and Han-Pu Liang*[abcd]

[a] Key Laboratory of Biofuels, Qingdao Institute of Bioenergy and Bioprocess Technology, Chinese Academy of Sciences, Qingdao 266101, China

[b] Center of Materials Science and Optoelectronics Engineering, University of Chinese Academy of Sciences, Beijing 100049, China

[c] Dalian National Laboratory for Clean Energy, Chinese Academy of Sciences, Dalian 116023, China

[d] Shandong Energy Institute, Qingdao 266101, China

* Corresponding author. E-mail address: lianghp@qibebt.ac.cn (Han-Pu Liang)

Theoretical models for the water dissociation and hydrogen desorption

To investigate the effect of encapsulated Ni nanoparticles in the incomplete graphite layer on water dissociation and hydrogen desorption, we constructed the Ni(111), Ni(200), Ni(220), Pt(111) and C@Ni models. For a reasonable repeated period, 3×3 supercells were used for Ni(111), Ni(200) and Pt(111) surfaces, as well as 2×3 supercells were used for the Ni(220) surface. Two layers of metal atoms on the surface were fully relaxed, while the remaining atomic layers were frozen during the calculation of water dissociation. In the case of the C@Ni model, the 3×3 supercells of graphene covers the 3×3 supercells of Ni(111), where the lattice mismatch between them is less than 0.5%. One graphene layer and two layers of metal atoms on the surface were fully relaxed, and the remaining three atomic layers were frozen during the calculation of Gibbs free energy of hydrogen adsorption.

The adsorption (E_{ad}), active (E_{act}) and reaction (E_{rea}) energies of water dissociation were calculated by following equations:

$$E_{ad} = E(H_2O*) - E(slab) - E(H_2O)$$

$$E_{act} = E(TS) - E(H_2O*)$$

$$E_{rea} = E(OH*+H*) - E(H_2O*)$$

where $E(slab)$ and $E(H_2O*)$ are the total energy of models before and after water adsorption. $E(H_2O)$ is the energy of water. $E(TS)$ is the energy of transition state of water dissociation. $E(OH*+H*)$ represents the total energy of models after water dissociation. Transition states were identified by the complete linear synchronous transit / quadratic synchronous transit (LST/QST) method, where the reactant and product configurations were the above models of water adsorption (H_2O*) and water dissociation ($OH*+H*$).

The Gibbs free energy of hydrogen adsorption ($\Delta G(H*)$) was calculated by the following equation:

$$\Delta G(H*) = \Delta E + \Delta ZPE - T\Delta S$$

in which, ΔE, ΔZPE and ΔS are the binding energy, zero point vibration energy change and entropy change of hydrogen adsorption, respectively. Among them, $\Delta E=[E(9H^*)-E(H^*)-4E(H_2)]/8$, where $E(9H^*)$ or $E(H^*)$ is the total energy of the model adsorbed by nine or one hydrogen atom, and $E(H_2)$ is the energy of single hydrogen molecule. Furthermore, $\Delta ZPE=ZPE(H^*)-1/2ZPE(H_2)$ is used to estimate zero point vibration energy change. It is noted that the $ZPE(H_2)$ value is about 0.264 eV, which is very close to the one (0.270 eV) reported by Norskov et al.[1] Additionally, $\Delta S=S(H^*)-1/2S(H_2)\approx-1/2S(H_2)$ is obtained due to the negligible vibrational entropy of hydrogen adsorbed on models. The $T\Delta S$ thus is −0.205 eV, in view of the case that $TS(H_2)$ is about 0.41 eV for H_2 at 298 K and 1.0 atm.
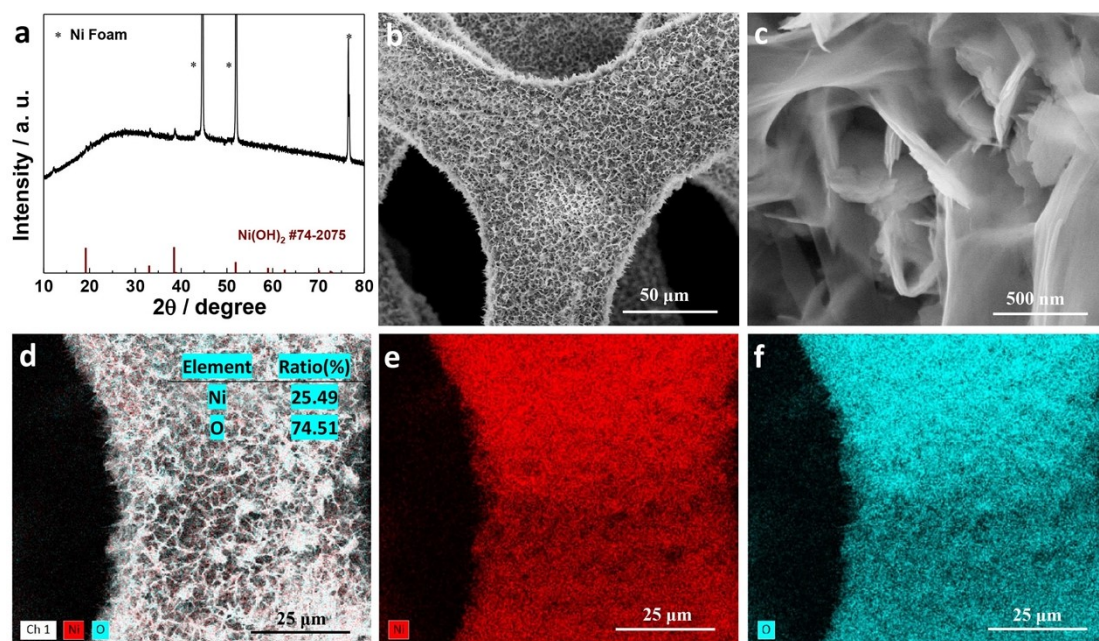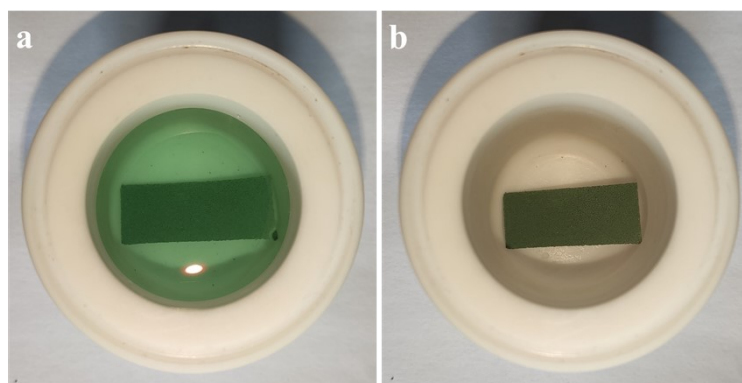
Fig. S1 (a) The XRD pattern and (b and c) SEM images of $Ni(OH)_2$ grown on a Ni foam fabricated at 160 °C for 3 h in an oven. (d-f) The corresponding EDS mapping images of Ni and O. The inset in (d) shows their atomic ratio.
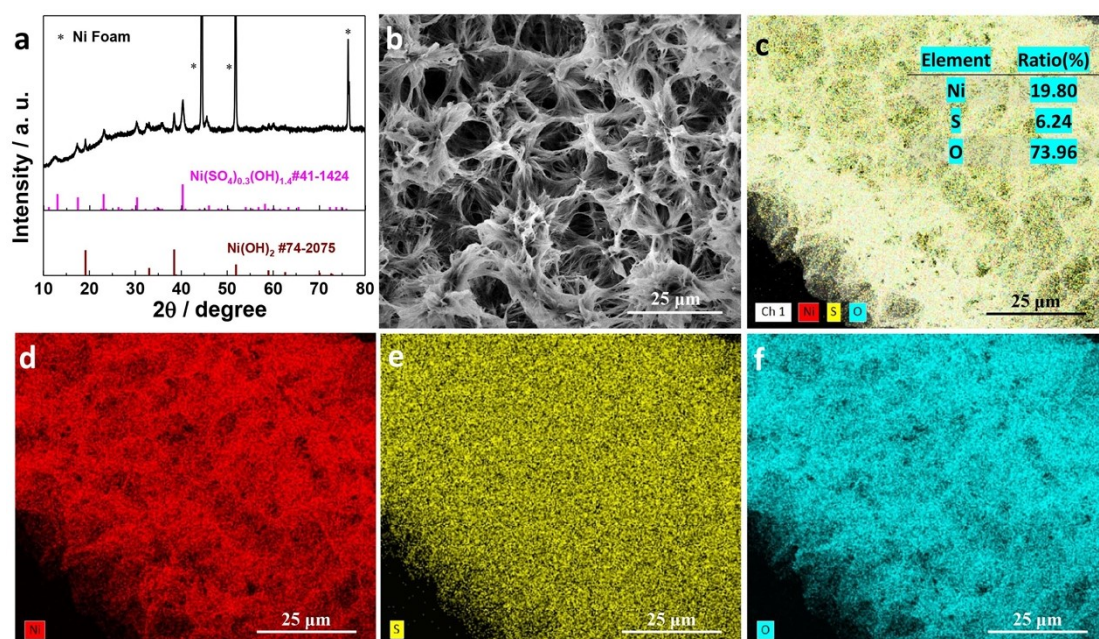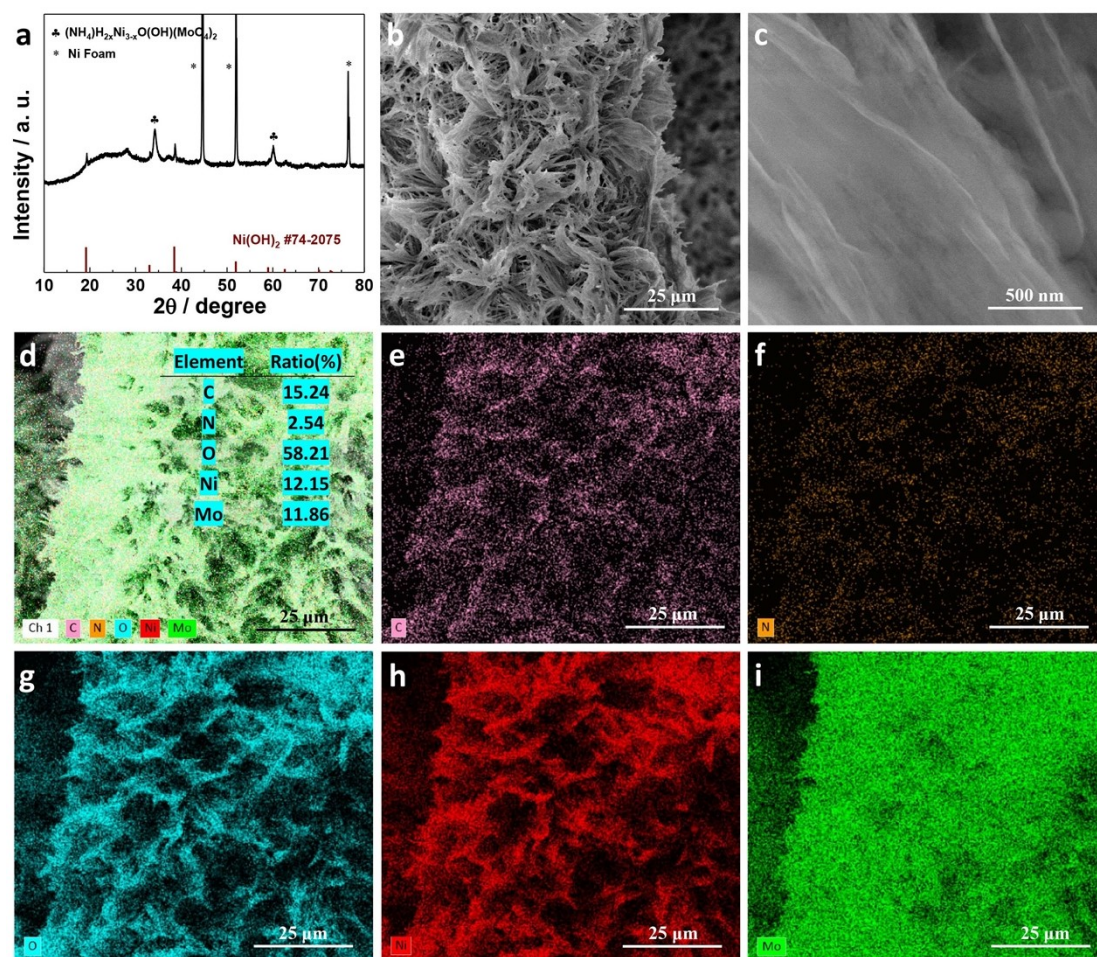

Fig. S2 (a) The XRD pattern and (b) SEM image of $Ni(SO_4)_{0.3}(OH)_{1.4}$-$Ni(OH)_2$ grown on a Ni foam fabricated at 160 °C for 12 h in an oven. (c-f) The corresponding EDS mapping images of Ni, S and O. The inset in (c) shows their atomic ratio.

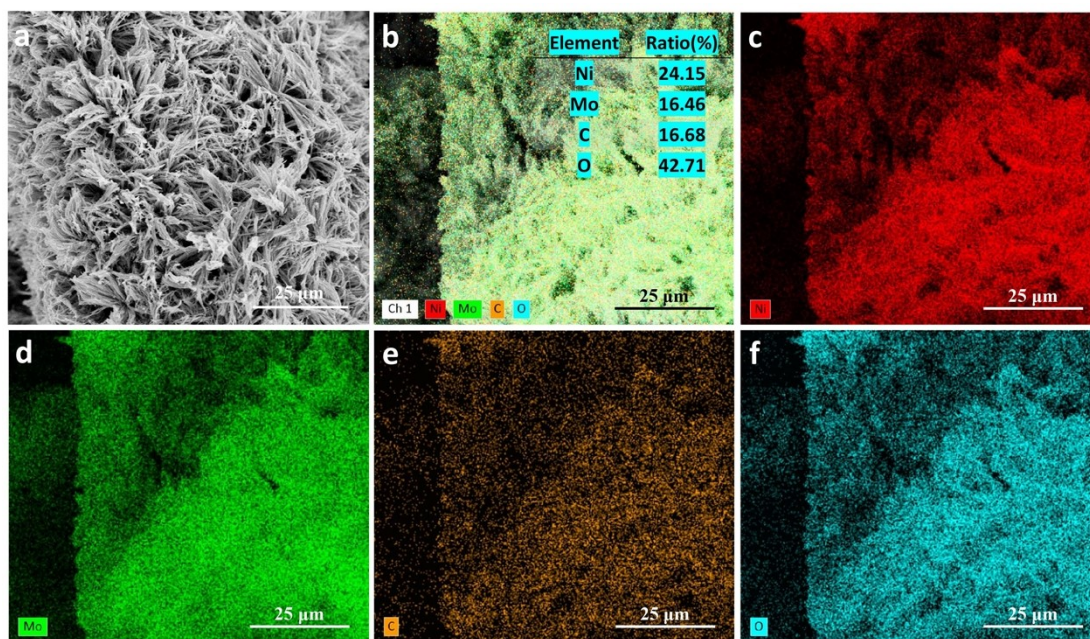**Fig. S3** Optical images of the $Ni(SO_4)_{0.3}(OH)_{1.4}$-$Ni(OH)_2$ grown on a Ni foam fabricated at 160 °C after 12 h in an oven (a) with and (b) without solution.
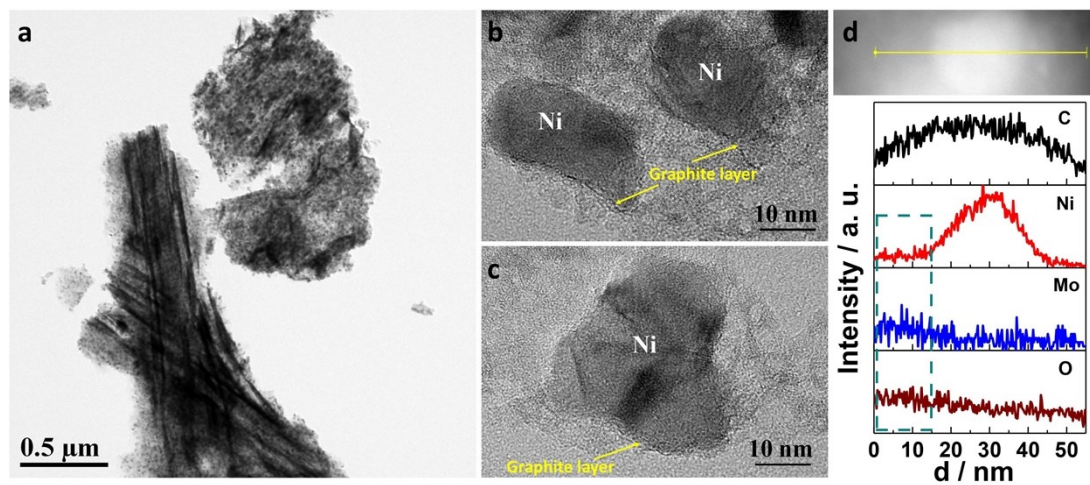

Fig. S4 (a) The XRD pattern and (b and c) SEM images of $C@(NH_4)H_{2x}Ni_{3-x}O(OH)(MoO_4)_2$-$Ni(OH)_2$ grown on a Ni foam fabricated at 170 °C for 12 h in an oven. (d-i) The corresponding EDS mapping images of C, N, O, Ni and Mo. The inset in (d) shows their atomic ratio.
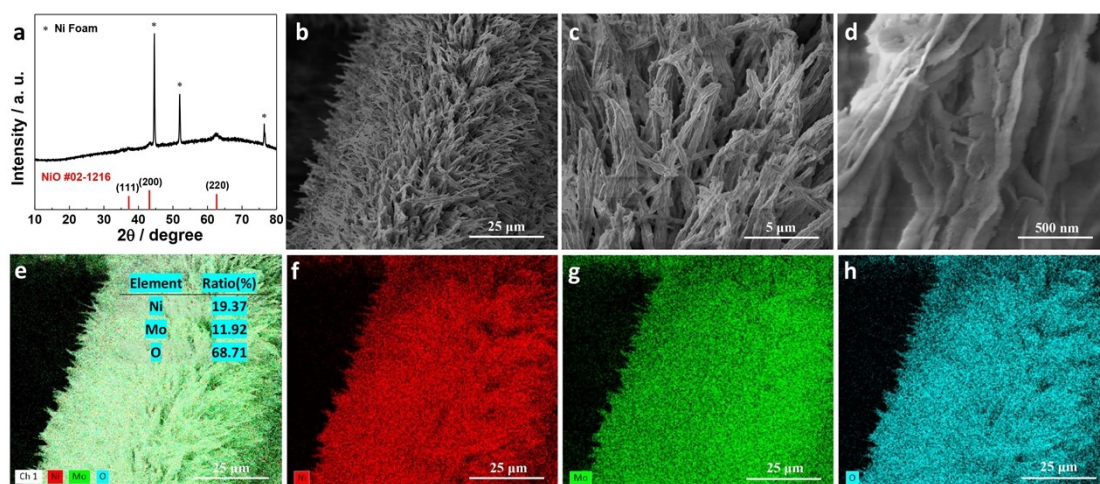
Fig. S5 (a) The SEM image of IG@Ni-NiMoO$_x$. (b-f) The corresponding EDS mapping images of Ni, Mo, C and O. The inset in (b) shows their atomic ratio.

Element	Ratio(%)
Ni	24.15
Mo	16.46
C	16.68
O	42.71

Fig. S6 (a) TEM and (b and c) HRTEM images of IG@Ni-NiMoO$_x$. (d) EDS line-scanning curves of IG@Ni-NiMoO$_x$.
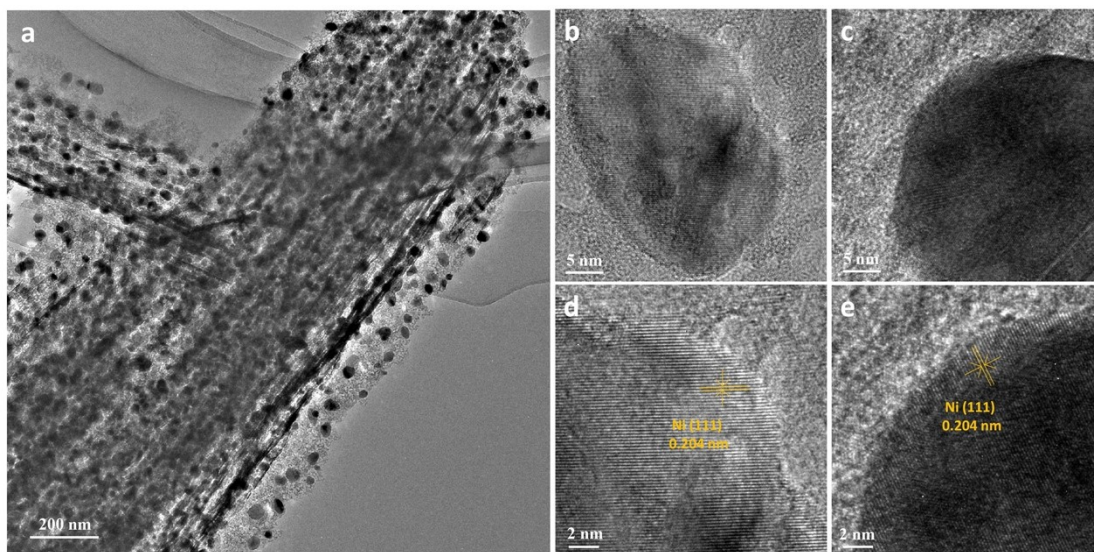
Fig. S7 (a) The XRD pattern and (b-d) SEM images of NiMoO$_x$. (e-h) The corresponding EDS mapping images of Ni, Mo and O. The inset in (e) shows their atomic ratio.
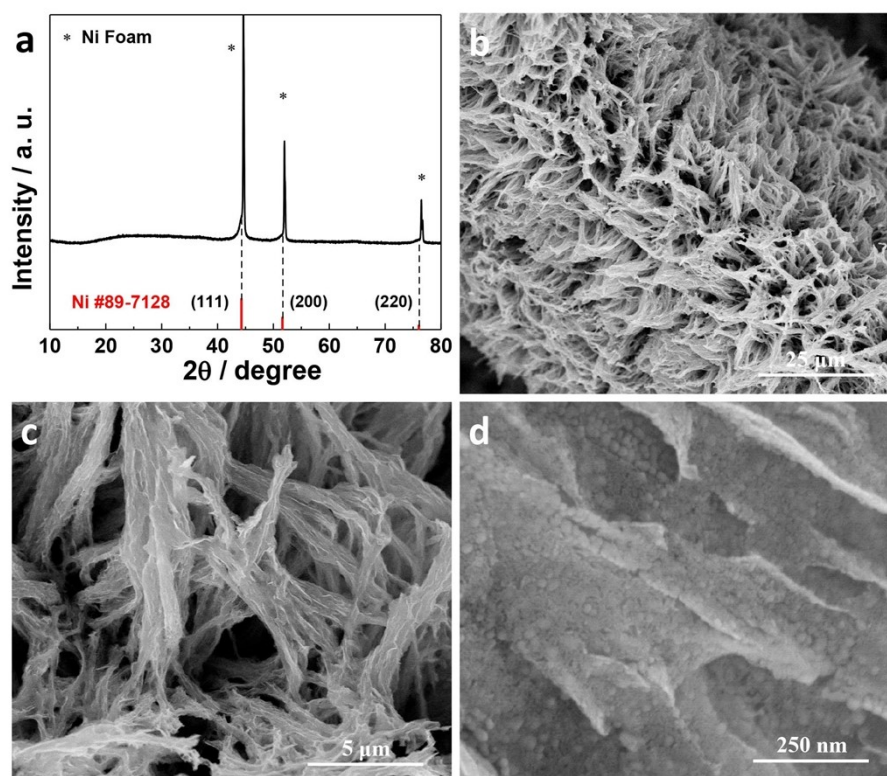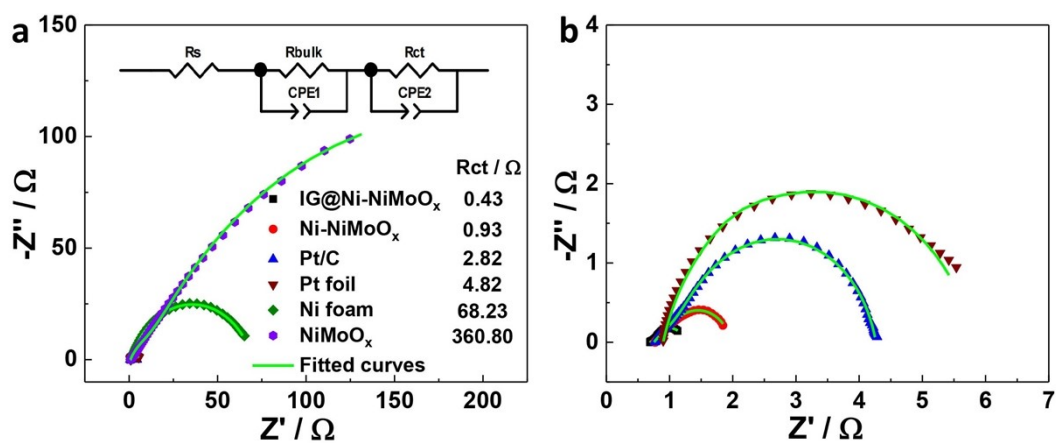

Fig. S8 (a) The XRD pattern and (b-d) SEM images of Ni-NiMoO$_x$ fabricated in the absence of glucose.

Fig. S9 (a) TEM and (b-e) HRTEM images of Ni-NiMoO$_x$.

Fig. S10 (a) Nyquist plots of all the investigated catalysts at −50 mV versus RHE and the corresponding fitted curves in 1 M KOH aqueous solution. (b) Nyquist plots of IG@Ni-NiMoO$_x$, Ni-NiMoO$_x$, Pt/C and Pt foil and the corresponding fitted curves. The inset in (a) shows the equivalent electric circuit and charge-transfer resistances (Rct) of all the investigated catalysts.
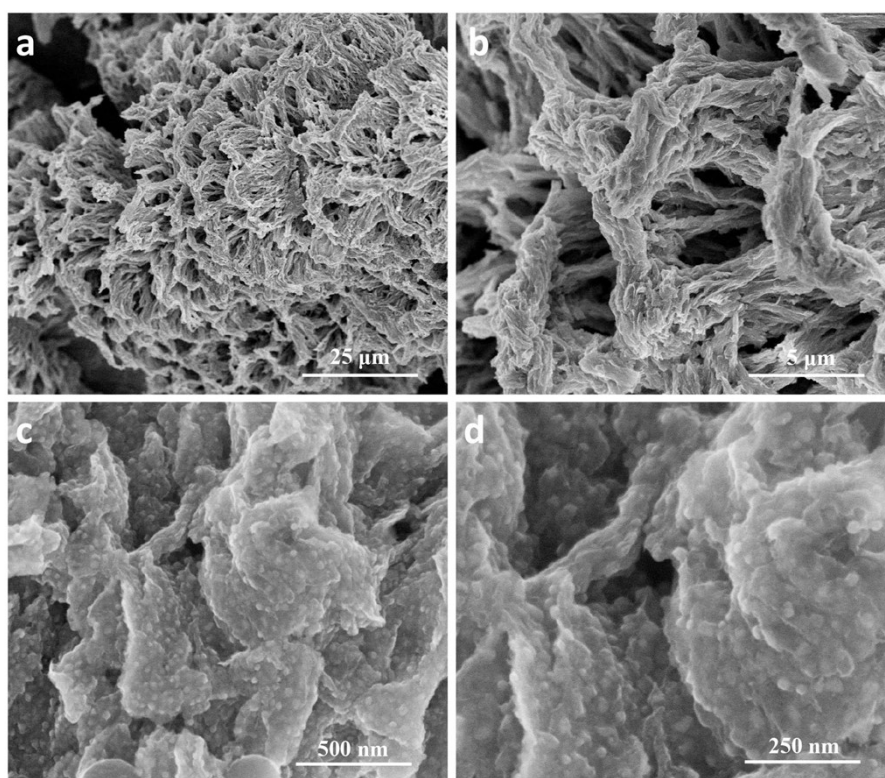
Fig. S11 (a-d) SEM images of IG@Ni-NiMoO$_x$ after stability tests at different magnifications.
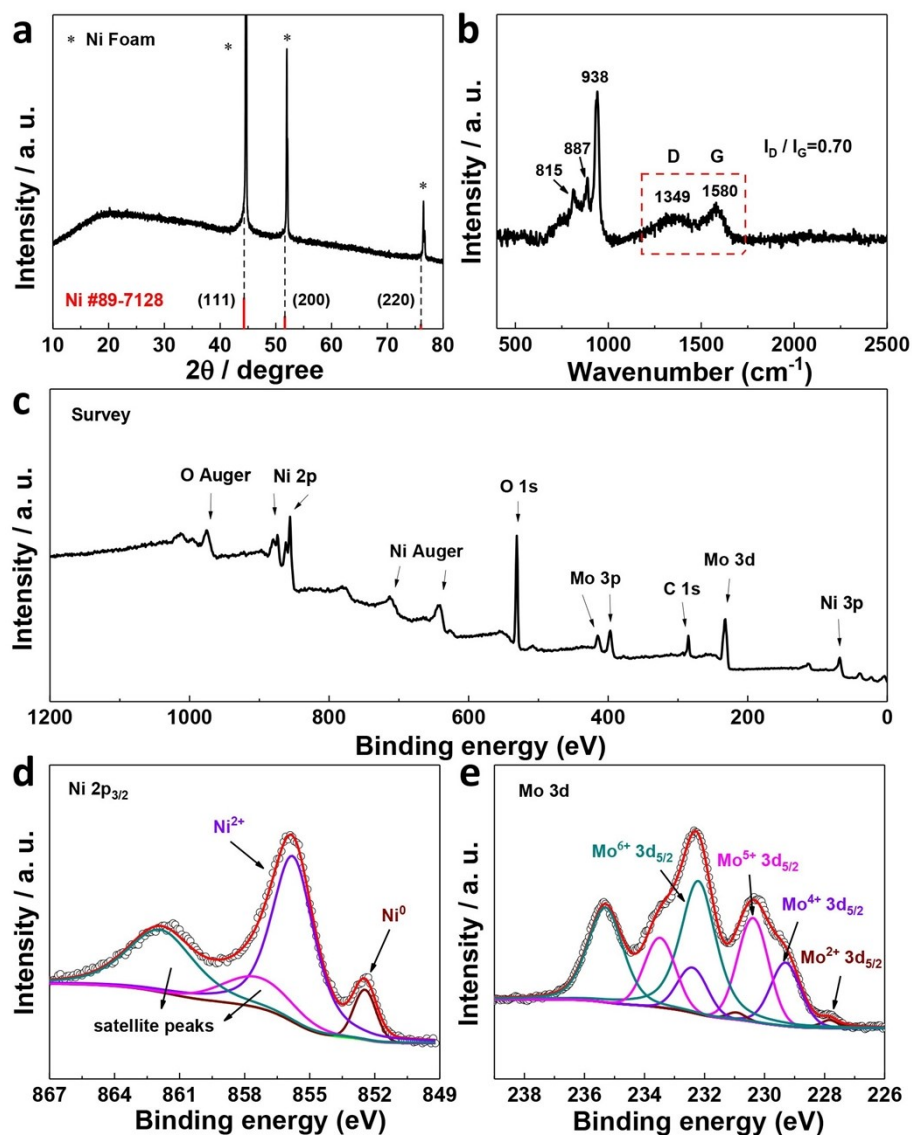
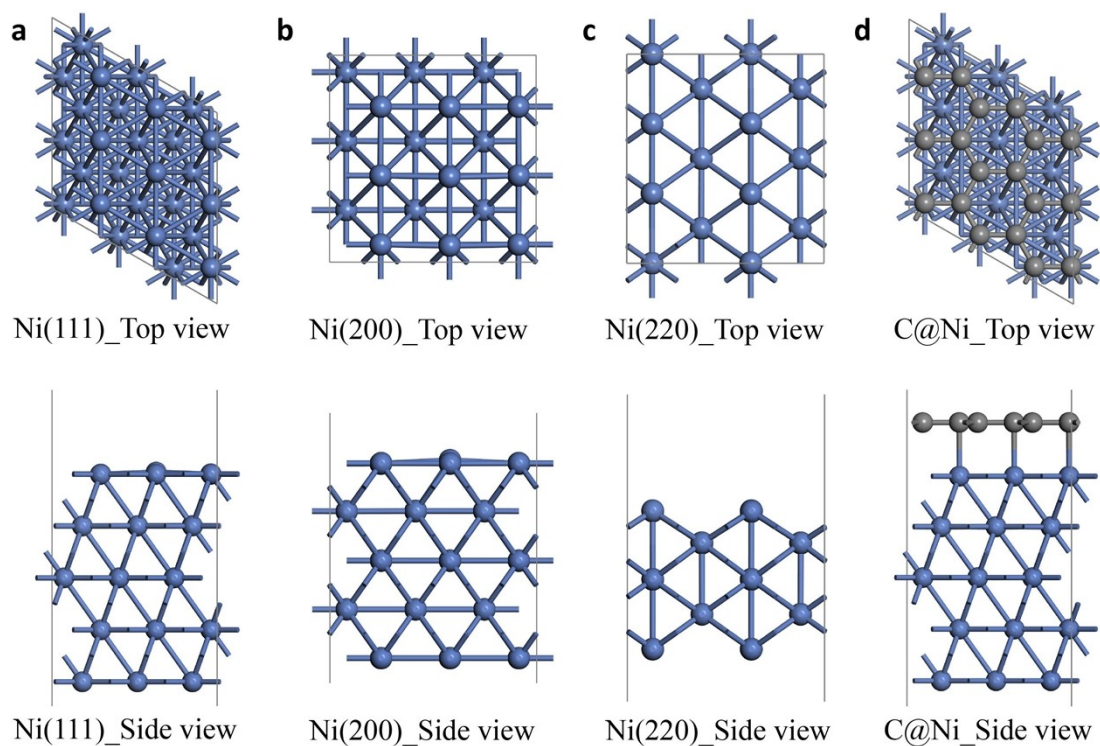**Fig. S12** (a) The XRD pattern and (b) Raman spectrum of IG@Ni-NiMoO$_x$ after stability tests. (c) Survey and high-resolution XPS spectra of (d) Ni 2p$_{3/2}$ and (e) Mo 3d of IG@Ni-NiMoO$_x$ after stability tests.

Fig. S13 (a-d) The top and side views of Ni(111), Ni(200), Ni(220) and C@Ni surfaces, in which the blue and grey spheres denote the Ni and C atoms.

IS   TS   FS
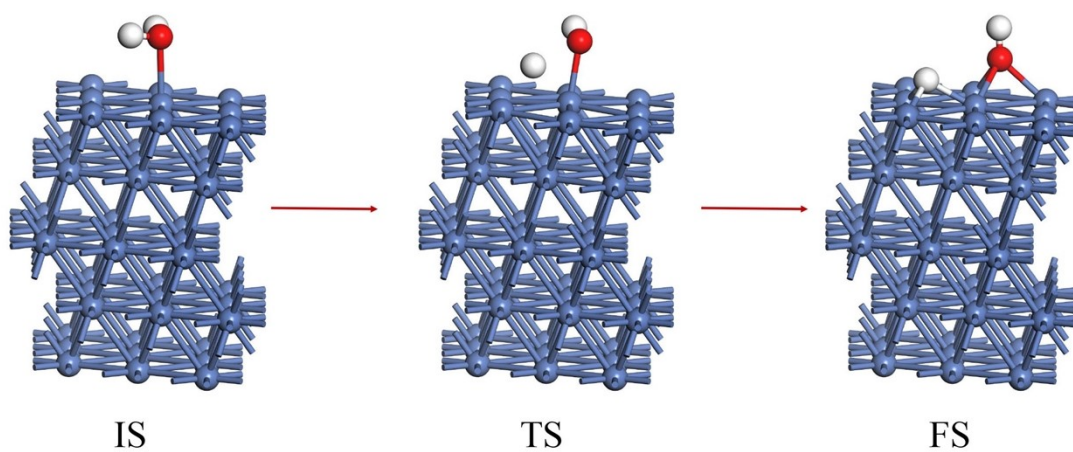
Fig. S14 Schematic diagram of water dissociation for the Ni(111) surface, in which the blue, red and white spheres denote the Ni, O and H atoms.
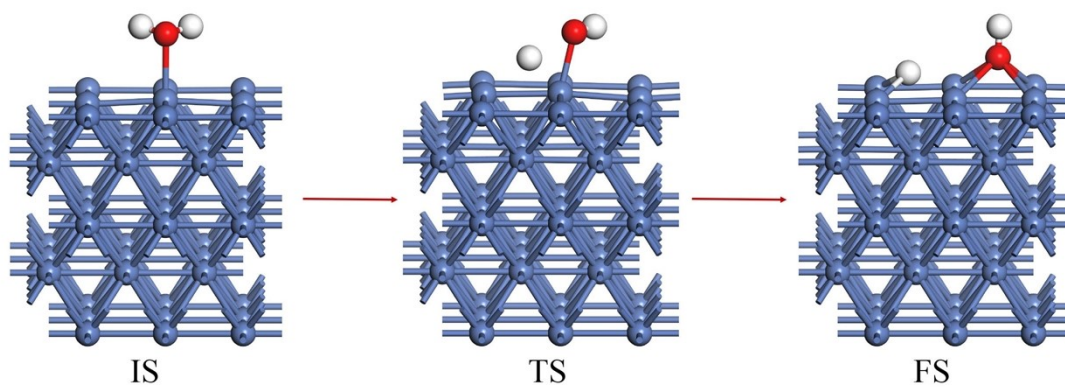
Fig. S15 Schematic diagram of water dissociation for the Ni(200) surface, in which the blue, red and white spheres denote the Ni, O and H atoms.

Fig. S16 Schematic diagram of water dissociation for the Pt(111) surface, in which the dark green, red and white spheres denote the Pt, O and H atoms.

Table S1 Atomic ratios of catalysts from XPS.

	Ni	Mo	O	C
IG@Ni-NiMoO$_x$	9.40	15.31	47.07	28.22

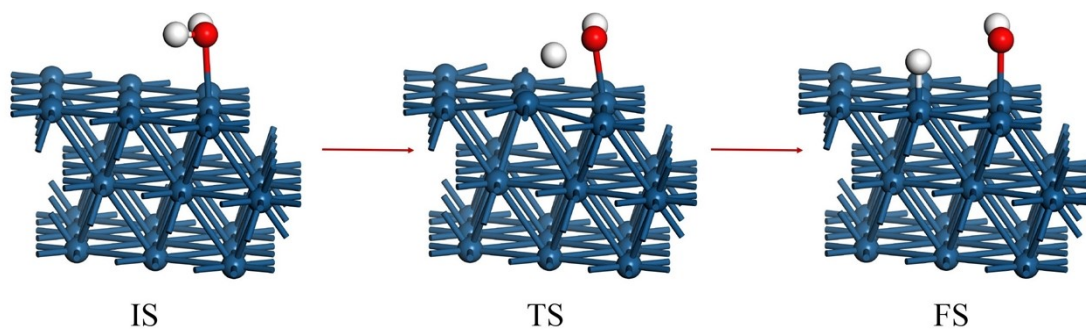**Table S2** Comparison of representative HER catalysts in 1 M KOH aqueous solution.

Catalyst	Current (mA cm^{-2})	Overpotential (mV)	Tafel Slope (mV dec^{-1})	ref
Ni-NiMoO$_x$	−10	61.88	62.59	This work
	−100	123.72		
IG@Ni-NiMoO$_x$	−10	44.35	39.88	
	−100	76.70		
Pt foil	−10	74.02	58.01	
	−100	159.91		
Pt/C	−10	56.49	51.81	
	−100	209.30		
Ni foam	−10	245.29	91.35	
	−100	358.00		
NiMoO$_x$	−10	221.62	102.03	
	−100	350.09		
Ni-Mo$_2$C@NPC	−100	260	64	[2]
Cu NDs/Ni$_3$S$_2$ NTs-CFs	−100	265	76	[3]
Ni$_5$Co$_3$Mo-OH	−100	245	59	[4]
Ni-Mo-N/CFC	−100	240	70	[5]
Ni$_3$N-VN/NF	−100	218	37	[6]
NiMoCo	−100	115	34	[7]
Ni/Mo$_2$C-NCNFs	−100	195	58	[8]
Ni-FeP/C	−100	160	72	[9]
Ni/Ni(OH)$_2$	−100	155	53	[10]
NiSe$_2$/Ni$_3$Se$_4$/NF	−100	228	70	[11]

Table S3 Water adsorption on top sites of Ni and Pt surfaces: Z_O (Å) is the height of O atom in water above the slabs, d_{O-H} (Å) is the distance between oxygen and hydrogen atoms, the angle (∘) is the angle of water and E_{ad} (eV) is the adsorption energy of water.

Surface	Z_O (Å)	d_{O-H} (Å)	Angle (°)	E_{ad} (eV)
Pt(111)	2.320	0.988, 0.988	104.426	−0.294
Ni(111)	2.140	0.988, 0.989	104.592	−0.556
Ni(200)	2.101	0.988, 0.988	105.320	−0.622
Ni(220)	2.097	0.986, 0.986	105.182	−0.645

References

1   J. K. Norskov, T. Bligaard, A. Logadottir, J. R. Kitchin, J. G. Chen, S. Pandelov and U. Stimming, *J. Electrochem. Soc.*, 2005, **152**, J23-J26.

2   Y. K. Lu, C. L. Yue, Y. P. Li, W. J. Bao, X. X. Guo, W. F. Yang, Z. Liu, P. Jiang, W. F. Yan, S. J. Liu, Y. Pan and Y. Q. Liu, *Appl. Catal., B*, 2021, **296**, 120336.

3   J.-X. Feng, J.-Q. Wu, Y.-X. Tong and G.-R. Li, *J. Am. Chem. Soc.*, 2020, **142**, 18997-18997.

4   S. Y. Hao, L. C. Chen, C. L. Yu, B. Yang, Z. J. Li, Y. Hou, L. C. Lei and X. W. Zhang, *ACS Energy Lett.*, 2019, **4**, 952-959.

5   Y. Li, X. F. Wei, L. S. Chen, J. L. Shi and M. Y. He, *Nat. Commun.*, 2019, **10**, 5335.

6   H. J. Yan, Y. Xie, A. P. Wu, Z. C. Cai, L. Wang, C. G. Tian, X. M. Zhang and H. G. Fu, *Adv. Mater.*, 2019, **31**, 1901174.

7   K. L. Hu, M. X. Wu, S. Hinokuma, T. Ohto, M. Wakisaka, J.-i. Fujita and Y. Ito, *J. Mater. Chem. A*, 2019, **7**, 2156-2164.

8   M. X. Li, Y. Zhu, H. Y. Wang, C. Wang, N. Pinna and X. F. Lu, *Adv. Energy Mater.*, 2019, **9**, 1803185.

9   X. F. Lu, L. Yu and X. W. Lou, *Sci. Adv.*, 2019, **5**, eaav6009.

10 L. Dai, Z.-N. Chen, L. X. Li, P. Q. Yin, Z. Q. Liu and H. Zhang, *Adv. Mater.*, 2020, **32**, 1906915.

11 L. Tan, J. T. Yu, H. Y. Wang, H. T. Gao, X. Liu, L. Wang, X. L. She and T. R. Zhan, *Appl. Catal., B*, 2022, **303**, 120915.